Journal of Renewable Materials
DOI:10.32604/jrm.2020.09573
Article

Tech Science Press

Axial Mechanical Properties of Timber Columns Subjected to Freeze-Thaw Cycles

Kang He[1], Yu Chen[1,*] and Jian Wang[2]

[1]College of Civil Engineering, Fuzhou University, Fuzhou, 350116, China
[2]School of Urban Construction, Yangtze University, Jingzhou, 434023, China
*Corresponding Author: Yu Chen. Email: kinkingingin@163.com
Received: 31 December 2019; Accepted: 18 May 2020

Abstract: The behaviour of timber columns subjected to freeze-thaw cycles under axial compression is presented in this paper. A total of forty specimens, including twenty circular timber columns and twenty square timber columns, were tested under axial compression. The failure modes, ultimate bearing capacity, ductility coefficient, load-displacement curves and load-strain curves were obtained and analyzed. The number of freeze-thaw cycles (from 0 to 80) and the specimens' height (from 225 mm to 360 mm) were considered as the main parameters. After freeze-thaw cycles, there was no obvious change on the surface of the timber columns. The test results showed that freeze-thaw cycles could reduce the ultimate bearing capacity of the timber columns, and the average reduction of the ultimate bearing capacity of the specimen reached 28%. The ductility coefficient of the square specimens subjected to freeze-thaw cycles almost remains constant compared with that of the square timber columns left untreated. While the ductility coefficient of the circular timber columns increases after freeze-thaw cycles. In addition, based on the extensive experimental analysis, a regression formula is derived to predict the ultimate bearing capacity of the timber columns after being subjected to freeze-thaw cycles, which is proved to be reasonable accurate.

Keywords: Timber columns; freeze-thaw cycles; axial mechanical property; ductility coefficient; regression formula

1 Introduction

Wood and bamboo are both renewable biomass material from a wide range of sources, both natural and cultivated. At the same time, wood and bamboo are environmentally friendly materials rich in natural cellulose, which plays a great supporting role in human production and life [1–3]. With the decrease of mineral resources, wood as a renewable resource has more obvious advantages and is widely used in the field of structural construction and interior decoration [4]. When wood is used as building material, moisture content and temperature are two important factors influencing its mechanical properties [5]. When the ambient temperature changes, the mechanical properties of the wood will change accordingly. In the existing research, the effect of high temperature on the mechanical properties of wood has been more mature [6–9]. However, studies on the effect of low temperature on mechanical properties of wood are relatively few.

With the exploration of materials in the field of low temperature, the influence of low temperature on wood properties has also been concerned. Kim et al. [10] studied the strength and stability of plywood at low temperatures, allowing it to act as a container for liquefied natural gas. Ayrilmis et al. [11,12] studied the mechanical properties of artificial wood panels under snow loads and low temperatures when used for roofing. Through experimental research, Gerhards et al. [13,14] found that the bending strength and elastic modulus of wood increased with the decrease of temperature at low temperature and were affected by water content. Gao et al. [15] tested the dynamic and static elastic modulus of the *Pinus resinosa* samples with different moisture content in the temperature range of –40°C to 40°C. The bearing capacity and stability of original bamboo columns and sprayed composite mortar-original bamboo composite columns were investigated through axial compression testing by Tian et al. [16]. Szmutku et al. [17] found that rapid cooling had little effect on mechanical properties, while slow cooling significantly reduced the mechanical properties of wood. The mechanical properties of wood in the natural environment decrease even more due to the multiple freezing-thawing cycles at the same time. Some studies have analyzed the reaction of free water, absorbed water and bound water in wood at low temperature from the micro point of view [18–21].

Many scholars have also carried out relevant research on the internal relationship between wood moisture content and its performance. Barrett et al. [22] showed through experiments that increases in member bending strength with moisture content will compensate for section property decreases at all bending strength property levels. The effects of chromated copper arsenate (CCA) treatment on lumber at or near 12% moisture content and at failure times of 1 to 10 min were evaluated by Winandy [23]. Kretschmann et al. [24,25] evaluated the effects of moisture content on the physical properties of specific wood strength and fracture toughness through experiments and numerical models. An empirical linear relationship was developed between dowel-bearing strength and moisture content using the first group of specimens by Rammer et al. [26], which compared favorably with results from the second group. The influence of wood moisture on bending modulus, bending strength and shear modulus G(zx) and G(zy) was determined through experimental research [27]. Sedano-Mendoza et al. [28] found that relative percentage of moisture content of surface and core layers in pine tannin-bonded particleboard influences markedly the internal bond strength of the board. Jiang et al. [29] verified by experiment that a distinct moisture dependency is exhibited for the elastic and strength behavior of Chinese fir wood. Experimental research conducted by Bader et al. [30] shown that for the best pliability during bending, the moisture content of longitudinally compressed wood must be close to its fiber saturation point. In this paper, the mechanical performance of timber columns subjected to freeze-thaw cycles were investigated. Moreover, a formula in calculating the ultimate bearing capacity of timber columns was derived according to the experiment results.

2 Experimental Program

2.1 Specimens Preparation

A total of forty specimens, including twenty circular timber columns and twenty square timber columns, were prepared. Besides, two timber columns were selected to put the thermometers in measuring the actual temperatures of specimens. Since the internal dimensions of the rubber box of the rapid freeze-thaw testing equipment are 105 mm × 105 mm × 500 mm, the outer width of square timber columns and the diameter of circular timber columns are designed as 90 mm. The main parameters are shown as follows:

- Height of timber columns (H): 225 mm, 270 mm, 315 mm and 360 mm.
- Number of freeze-thaw cycles (N): 0, 20, 40, 60 and 80.

2.2 Specimens Labeling

All specimens are labeled in accordance with the section types, the height of the timber columns and the number of freeze-thaw cycles. The details of all specimens are presented in Tab. 1. Using ‘S-H225-N20’ as an example, it was defined as follows:

Table 1: Details of all specimens

Section type	Labels	H (mm)	N	D (mm)
Square	S-H225-N0	225	0	90
	S-H225-N20	225	20	90
	S-H225-N40	225	40	90
	S-H225-N60	225	60	90
	S-H225-N80	225	80	90
	S-H270-N0	270	0	90
	S-H270-N20	270	20	90
	S-H270-N40	270	40	90
	S-H270-N60	270	60	90
	S-H270-N80	270	80	90
	S-H315-N0	315	0	90
	S-H315-N20	315	20	90
	S-H315-N40	315	40	90
	S-H315-N60	315	60	90
	S-H315-N80	315	80	90
	S-H360-N0	360	0	90
	S-H360-N20	360	20	90
	S-H360-N40	360	40	90
	S-H360-N60	360	60	90
	S-H360-N80	360	80	90
Circular	C-H225-N0	225	0	90
	C-H225-N20	225	20	90
	C-H225-N40	225	40	90
	C-H225-N60	225	60	90
	C-H225-N80	225	80	90
	C-H270-N0	270	0	90
	C-H270-N20	270	20	90
	C-H270-N40	270	40	90
	C-H270-N60	270	60	90
	C-H270-N80	270	80	90
	C-H315-N0	315	0	90
	C-H315-N20	315	20	90
	C-H315-N40	315	40	90
	C-H315-N60	315	60	90
	C-H315-N80	315	80	90

(Continued)

Table 1 (continued).

Section type	Labels	*H* (mm)	*N*	*D* (mm)
	C-H315-N0	360	0	90
	C-H360-N20	360	20	90
	C-H360-N40	360	40	90
	C-H360-N60	360	60	90
	C-H360-N80	360	80	90

- The first letter 'S' denotes the section type of specimens is square.
- The second part of the label 'H225' denotes the nominal height of the timber column is 225 mm.
- The last part of the label 'N20' denotes the number of freeze-thaw cycles is 20.

2.3 Physical Parameters of Wood

The Russia pinus sylvestris were used in this paper, and considering the large variability of the timber, enough test samples were selected for statistical analysis. Indexes such as moisture content, air-dry density, the compression strength parallel to grain (fc) and elasticity modulus (E) were tested respectively. Sample size, specimen size and test results are shown in Tab. 2.

Table 2: Test results of physical parameters

Physical parameters	Average value	Coefficient of variation (%)	Specimen size (chordwise × radial × longitudinal)	Sample size
Moisture content	11.4%	2.3	20 mm × 20 mm × 20 mm	25
Air-dry density	0.434 g/cm^3	15.2	20 mm × 20 mm × 20 mm	25
Compression strength parallel to grain (f_c)	13.0 MPa	17.1	20 mm × 20 mm × 30 mm	35
Elasticity modulus (E)	9238 MPa	19.4	20 mm × 20 mm × 30 mm	35

2.4 Freeze-Thaw Tests

The construction industry standard of the People's Republic of China (JG/T243-2009) [31] was also adopted in this test to set the parameters of the apparatus of rapid freeze-thaw cycles. The schematic diagram of the rapid freeze-thaw testing equipment is shown in Fig. 1. The temperature at the center of the timber columns ranged from –20°C to 20°C.

In the test, the rapid freeze-thaw cycles equipment just simulated a process of freeze-thaw cycles for the timber columns since there is no definite standard for the timber columns subjected to freeze-thaw cycles. Thirty-two timber columns, including 16 circular specimens and 16 square specimens, were exposed to freeze-thaw cycles. The rest eight timber columns were left untreated at ambient temperature. It must be mentioned that freeze-thaw cycles in this test were closely related to the change of temperature of water. Since water seasoning could indirectly make the timber columns subject to freeze-thaw cycles, the water seasoning was not adopted on the specimens left untreated at ambient temperature in order to eliminate the effect of water as far as possible.

Owing to the fact that the quality of the timber columns is smaller than buoyancy from the water, the steel discs whose dimension was designed to be 90 mm × 90 mm × 25 mm was used to ensure that the

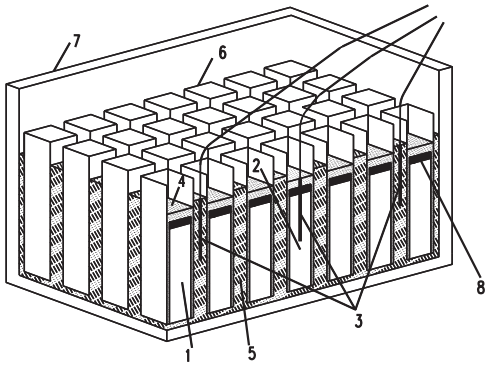

Figure 1: Schematic diagram of the rapid freeze-thaw test
1—Specimens; 2—The specimen for temperature measurement; 3—Thermocouples; 4—Water; 5—Antifreeze fluid; 6—Rubber box; 7—Container; 8—Steel disc

timber columns were fully surrounded by water. Besides, the changes, including the shape, the grain and the original crack of the timber columns subjected to freeze-thaw cycles, were observed after the freeze-thaw cycles. It was found that the freeze-thaw cycles had little effect on the shape and the grain of the timber columns. The changes of the original crack of the timber columns had been quite consistent with the transition between freeze-thaw cycles: The original crack became smaller gradually when the specimens were subjected to the process of freezing. The original crack became larger slowly when the process of thawing was carried out. As a result, the changes of original crack were not happened to the timber columns after being exposed to freeze-thaw cycles.

2.5 Compression Test

After the freeze-thaw cycles and the dry treatment were finished, a hydraulic universal testing machine of 1000 kN capacity, as shown in Fig. 2a, was used to carry out compression tests on the timber columns. At the meantime, the strain test was executed on eight square timber columns (S-H225-N40, S-H270-N0, S-H270-N20, S-H270-N40, S-H270-N60, S-H270-N80, S-H315-N40, S-H360-N40) and eight circular timber columns (C-H225-N80, C-H270-N0, C-H270-N20, C-H270-N40, C-H270-N60, C-H270-N80, C-H315-N80, C-H360-N80) to gain the relationship between the load and strain by an automatic data acquisition system, called DH3816, which is shown in Fig. 2b. Four strain gauges (ε1-ε4) were attached at critical points on each square timber columns to gain the strain development. Two strain gauges (ε1-ε2) were placed at the mid-height of the square timber columns to obtain the transverse and longitudinal strain, respectively. Besides, another two strain gauges (ε3-ε4) were positioned at one side of the corner of the square timber columns to gain the strain in the transverse and longitudinal direction. As for circular timber columns, two strain gauges (ε5-ε6) were arranged in each circular timber columns used for strain

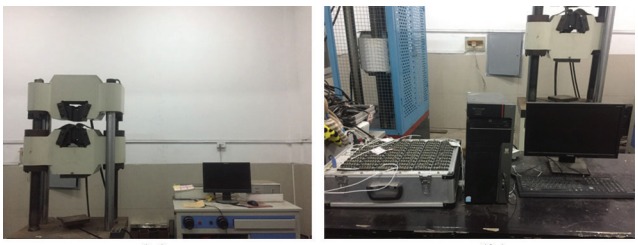

(a) (b)

Figure 2: The apparatus for axial pressure test. (a) Hydraulic universal testing machine. (b) Strain automatic acquisition system

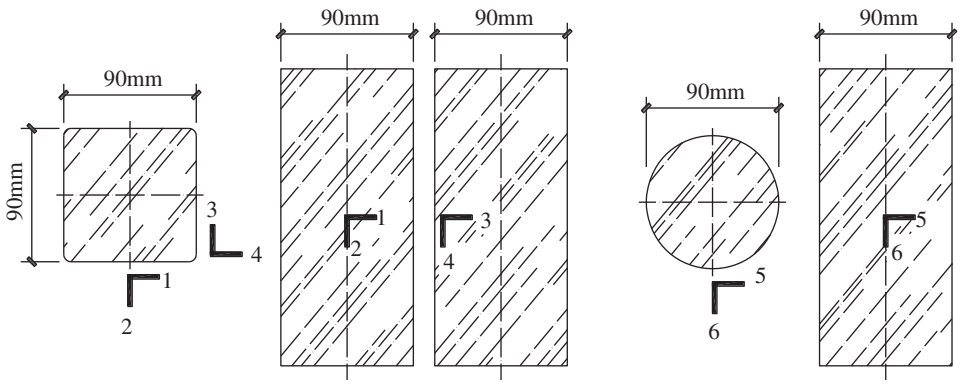

Figure 3: Arrangement of stain gauges. (a) Square specimens. (b) Circular specimens

test: both of two strain gauges were positioned at the center of the specimens, in which two strain gauges were used for the measurement of transverse and longitudinal strain, respectively. The details of the arrangement of the strain gauges are shown in Figs. 3a and 3b.

Before the strain test, a timber column was connected to DH3816 as compensation, and the machine was subsequently adjusted until the value of the strain was in the range from –10 to +10 in order to ensure the balance of the strain gauges. Multi-stage loading was executed on the specimens to gain the value of strain in different load, in which the time left for each grade of loading was one to two minutes in order to gain stable load. Before loading, the test specimen is accurately placed at the exact center of the loading device platform for geometric centering to ensure that the column is under axial compression. During the manufacturing process of the test specimen, the upper and lower surfaces of the column end are polished so that the column end is definitely flat. In this way, we can effectively avoid uneven local force on the column end during the pressure test. This test adopts load control for loading, which is divided into two stages—pre-loading and loading. The maximum preload is 10% of the estimated ultimate load of specimens. In the pre-loading stage, the test specimen is first geometrically centered. The centering of the test specimen is assessed according to the readings of the displacement gauge and the strain gauge. The position of the specimen is regulated until it is physically centered, while ensuring that the data on the strain gauge and the displacement gauge reading are normal. During the loading stage, a variable loading rate is used, which is segmented at 70% of the estimated ultimate load. Before the load reaches 70% of the estimated ultimate load, the loading rate is 1 kN/s. After the load reaches 70%, the loading rate decreases to 0.5 kN/s. The loading process being monotonic, the test continues until the specimen is broken.

3 Test Result

3.1 Failure Modes

The failure modes of the timber columns under compression were observed and summarized. For the square timber columns, the failure modes could be divided into three types according to the failure phenomenon: oblique shear failure (mode one), combination of longitudinal penetrating cracking and oblique shear failure (mode two) and longitudinal penetrating cracking (mode three), respectively, as shown in Figs. 4a–4c. It could be found from Tab. 3 that the number of specimens of each failure mode is respectively 10 for mode one, 4 for mode two and 6 for mode three. In addition, among the 20 square columns, when the column height is 360 mm, four of the five specimens are failure mode three, and the

(a) (b) (c)

Figure 4: Failure modes of the square timber columns. (a) Mode one. (b) Mode two. (c) Mode three

proportion of failure mode three is significantly higher than other shorter specimens (225 mm, 270 mm, 315 mm), which could be seen from Tab. 3.

For circular timber columns, the failure modes could also be divided into three types: longitudinal penetrating cracking (mode one), central cracking (mode two) and combination of crush failure and longitudinal cracking (mode three), respectively, as shown in Figs. 5a–5c. The number of specimens of each failure mode was recorded to be 5 for mode one, 3 for mode two and 12 for mode three, respectively. The failure modes of the circular specimens are also found to transform from longitudinal penetrating cracking (mode one) to combination of crush failure and longitudinal cracking (mode three) with the increase of the specimen's height, as seen from Tab. 3. In addition, all specimens after compression tests are shown in Figs. 6a and 6b.

3.2 Load-Displacement Curves

The relationship between the load (P) and displacement (Δ) of the circular and square timber columns under axial compression are shown in Figs. 7 and 8. It could be found that freeze-thaw cycles has a remarkable influence on the ultimate bearing capacity of the timber columns subjected to freeze-thaw cycles when compared with that of the timber columns left untreated. The height of the timber columns is also observed to play an important role on the ultimate bearing capacity of the timber columns. Besides, the load-displacement curve of each specimen could be divided into three stages: elastic stage, elastic-plastic stage and descending stage, according to the characteristics of the curves.

In the elastic stage, the initial stiffness of the circular and square timber columns is obviously influenced by freeze-thaw cycles. Although the initial stiffness of the test piece fluctuated after the freeze-thaw cycle, there was no consistent rule between the number of freeze-thaw cycles and the initial stiffness. The specimens' height has little effect on the initial stiffness of the timber columns, as can be seen from Figs. 7e–7h and 8e–8h.

When the applied loads reached to the yield load of the specimens, the timber columns started to enter into the elastic-plastic stage, in which stage the load-displacement curves of all specimens whether subjected to freeze-thaw cycles or not has no change.

As shown in Figs. 7 and 8, the curves of the timber columns entered into the descending stage when the load is up to the ultimate bearing capacity. It could be found that the ductility of the specimens subjected to freeze-thaw cycles is almost greater than that of the specimens without being exposed to freeze-thaw cycles

Table 3: The results of all specimens after compression tests

Labels	N_u (kN)	*Per*	Δ_u (mm)	N_y (kN)	Δ_y (mm)	$\mu = \Delta_u/\Delta_y$	Failure mode
S-H225-N0	155.55	0.0%	7.359	151.00	6.680	1.102	Mode one
S-H225-N20	106.65	31.4%	11.310	96.45	5.524	2.047	Mode one
S-H225-N40	109.50	29.6%	4.617	99.85	3.413	1.353	Mode one
S-H225-N60	119.25	23.3%	12.329	112.10	5.497	2.243	Mode one
S-H225-N80	99.10	36.3%	7.591	98.40	7.164	1.060	Mode one
S-H270-N0	189.75	0.0%	8.216	169.95	5.497	1.495	Mode one
S-H270-N20	107.15	43.5%	6.704	98.75	4.584	1.462	Mode one
S-H270-N40	109.20	42.5%	9.113	103.75	7.567	1.204	Mode two
S-H270-N60	89.95	52.6%	4.788	81.80	3.441	1.391	Mode three
S-H270-N80	99.15	47.7%	11.189	89.75	8.857	1.263	Mode one
S-H315-N0	158.55	0.0%	10.776	148.65	8.239	1.308	Mode one
S-H315-N20	123.35	22.2%	15.263	119.30	11.976	1.274	Mode one
S-H315-N40	119.35	24.7%	7.109	107.60	4.905	1.449	Mode two
S-H315-N60	125.75	20.7%	13.145	122.75	11.733	1.120	Mode two
S-H315-N80	124.10	21.7%	5.766	118.00	4.476	1.288	Mode three
S-H360-N0	144.70	0.0%	5.373	137.75	3.455	1.555	Mode two
S-H360-N20	133.75	7.6%	5.917	128.85	4.691	1.261	Mode three
S-H360-N40	126.70	12.4%	6.613	123.00	6.291	1.051	Mode three
S-H360-N60	137.70	4.8%	7.944	133.20	6.815	1.166	Mode three
S-H360-N80	132.10	8.7%	8.589	128.45	7.433	1.155	Mode three
C-H225-N0	162.35	0.0%	6.482	162.10	6.384	1.015	Mode one
C-H225-N20	167.85	–3.4%	6.360	158.20	4.852	1.311	Mode one
C-H225-N40	119.45	26.4%	7.258	114.85	6.169	1.176	Mode one
C-H225-N60	133.40	17.8%	13.065	121.80	4.785	2.730	Mode one
C-H225-N80	107.65	33.7%	9.829	99.30	4.677	2.101	Mode one
C-H270-N0	169.00	0.0%	6.926	159.95	5.901	1.174	Mode two
C-H270-N20	150.35	11.0%	20.000	144.75	6.061	3.300	Mode three
C-H270-N40	129.35	23.5%	4.587	119.85	3.669	1.250	Mode two
C-H270-N60	139.20	17.6%	13.800	127.65	9.503	1.452	Mode three
C-H270-N80	120.00	29.0%	19.194	110.00	10.013	1.917	Mode three
C-H315-N0	198.95	0.0%	16.452	187.35	9.839	1.672	Mode three
C-H315-N20	140.20	29.5%	20.000	119.25	4.436	4.509	Mode three
C-H315-N40	137.10	31.1%	7.712	131.15	6.116	1.261	Mode three
C-H315-N60	119.90	39.7%	11.744	115.35	10.215	1.150	Mode three
C-H315-N80	115.6	41.9%	12.248	109.45	9.087	1.348	Mode three

Table 3 (continued).

Labels	N_u (kN)	*Per*	Δ_u (mm)	N_y (kN)	Δ_y (mm)	$\mu = \Delta_u/\Delta_y$	Failure mode
C-H360-N0	239.25	0.0%	10.433	217.55	7.595	1.374	Mode three
C-H360-N20	164.65	31.2%	8.861	159.60	7.420	1.194	Mode three
C-H360-N40	153.50	35.8%	14.869	138.20	6.815	2.182	Mode three
C-H360-N60	125.90	47.4%	10.776	120.35	7.379	1.460	Mode three
C-H360-N80	109.95	54.0%	9.688	107.90	8.360	1.159	Mode two

(a) (b) (c)

Figure 5: Failure modes of the circular timber columns. (a) Mode one. (b) Mode two. (c) Mode three

(a) (b)

Figure 6: Specimens after compression tests. (a) Square specimens. (b) Circular specimens

regardless of their section types, which could be proved by the fact that the descent rate of curves of the specimens subjected to freeze-thaw cycles in the descending stage are smaller than that of the specimens left untreated at ambient temperature.

It can be seen from Figs. 7 and 8 that the ultimate bearing capacity of the circular and square specimens after freeze-thaw cycle treatment has decreased significantly. Besides, it also could be found that the specimens' height has great effect on the ultimate bearing capacity. For the square timber columns, the specimens with the height of 360 mm has the greater ultimate bearing capacity than other specimens, and the ultimate bearing capacity of the specimens with the height of 225 mm or 270 mm are almost the same. As to the circular timber columns, the ultimate bearing capacity of the specimens increases with the increasing of the height of the timber columns when the number of freeze-thaw cycles are 0 and 40,

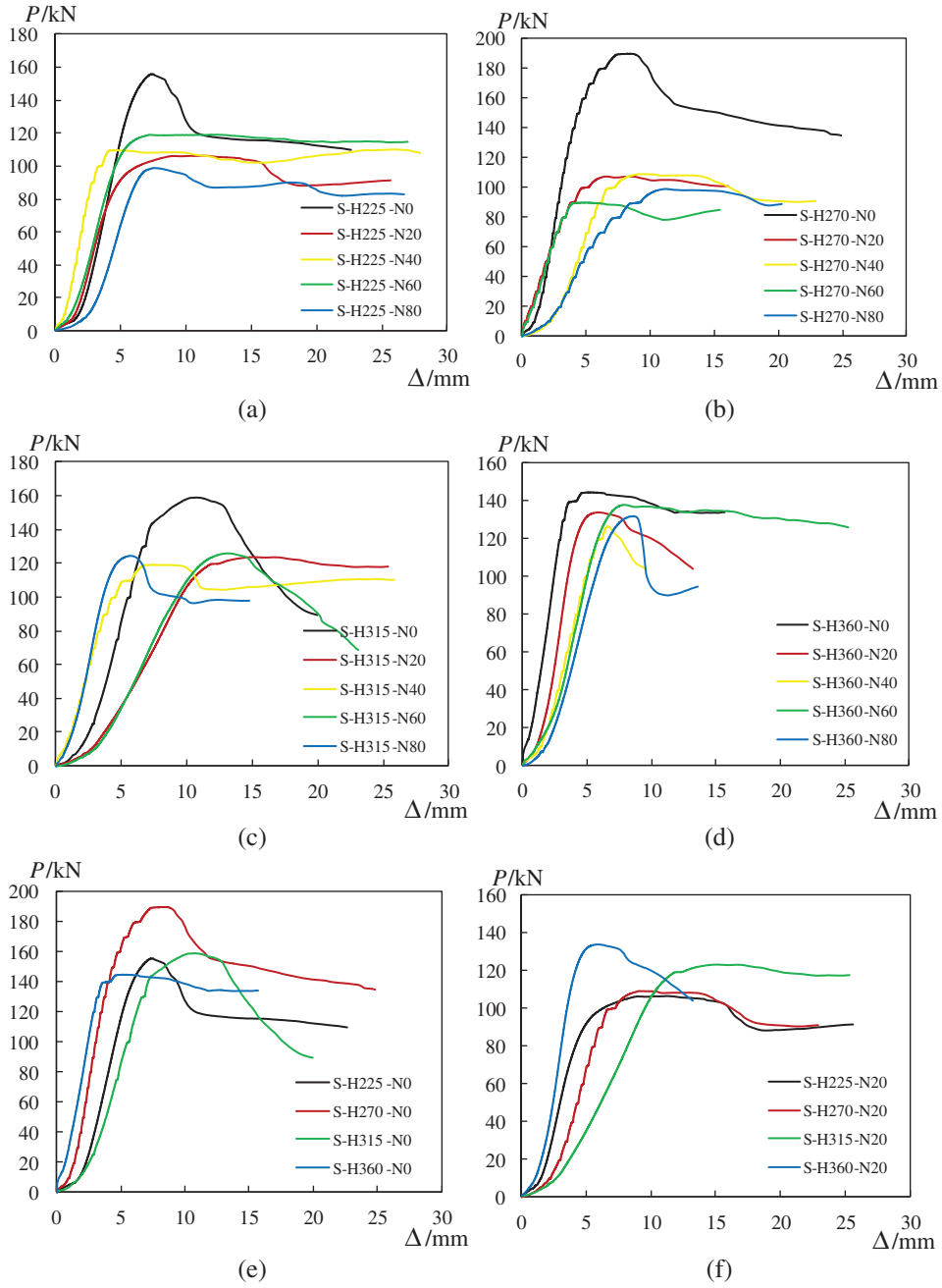

Figure 7: (continued)

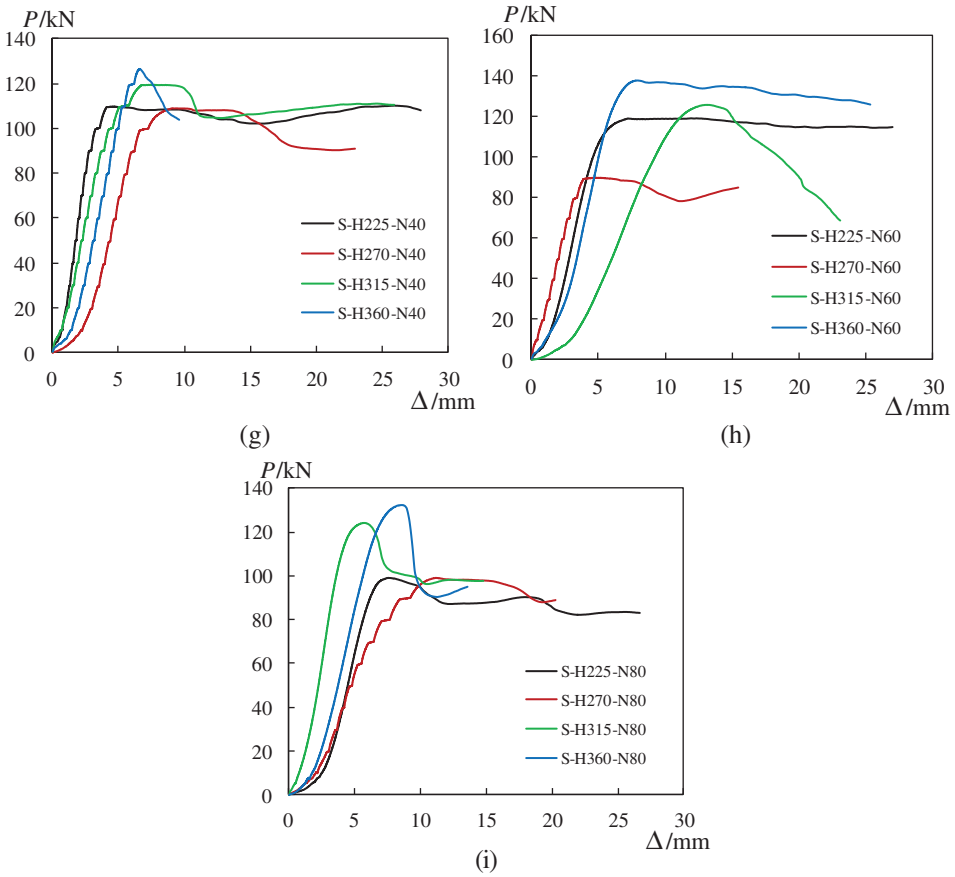

Figure 7: The load-displacement curves for square timber columns. (a) H = 225 mm. (b) H = 270 mm. (c) H = 315 mm. (d) H = 360 mm. (e) N = 0. (f) N = 20. (g) N = 40. (h) N = 60. (i) N = 80

which indicates that the number of freeze-thaw cycles has an important effect on the uptrend of the bearing capacity caused by the height of specimens.

3.3 Load-Strain Curves

The load-strain curves of different number of freeze-thaw cycles and specimens' height are shown in Figs. 9a–9c and 10a–10c, and the relationship between the load-strain curves and the points positioned in the square specimens for strain test are demonstrated in Fig. 9a. The level points of ε1 and ε3 are represented by the solid lines. The vertical points of ε2 and ε4 are represented by dotted lines; ε1 and ε2 are positioned at the center of the square specimens while ε3 and ε4 are positioned at the corner of the square specimens in accordance with the arrangement of the strain gauges in Fig. 3. As to the relationship between the load-strain curves and the points placed on the circular specimens, it is shown that the lever point of ε5 and the vertical point of ε6 are respectively represented by the solid and dotted line in Fig. 10a. Besides, each color of the line represents one of the specimens for strain test. In Figs. 9 and 10, the strain of the specimens for strain test increases with the increasing of the load.

The load-strain curves of the square timber columns subjected to different number of freeze-thaw cycles are shown in Fig. 9b. In the center area of the square specimens, the transverse and longitudinal strain of the specimen without being exposed to freeze-thaw cycles are respectively smaller than that of the specimens exposed to different number of freeze-thaw cycles at the same load levels. The maximum value of the

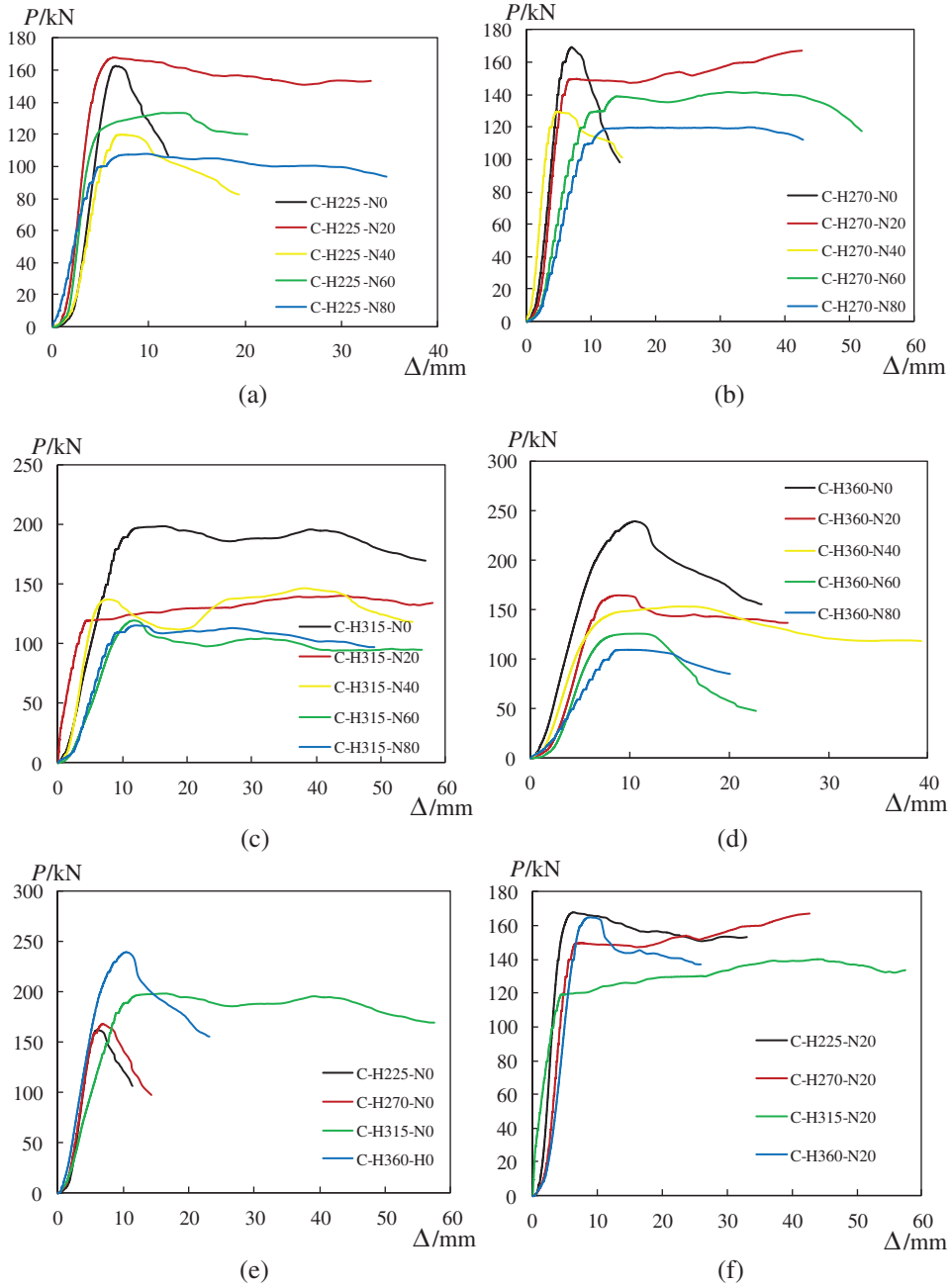

Figure 8: (continued)

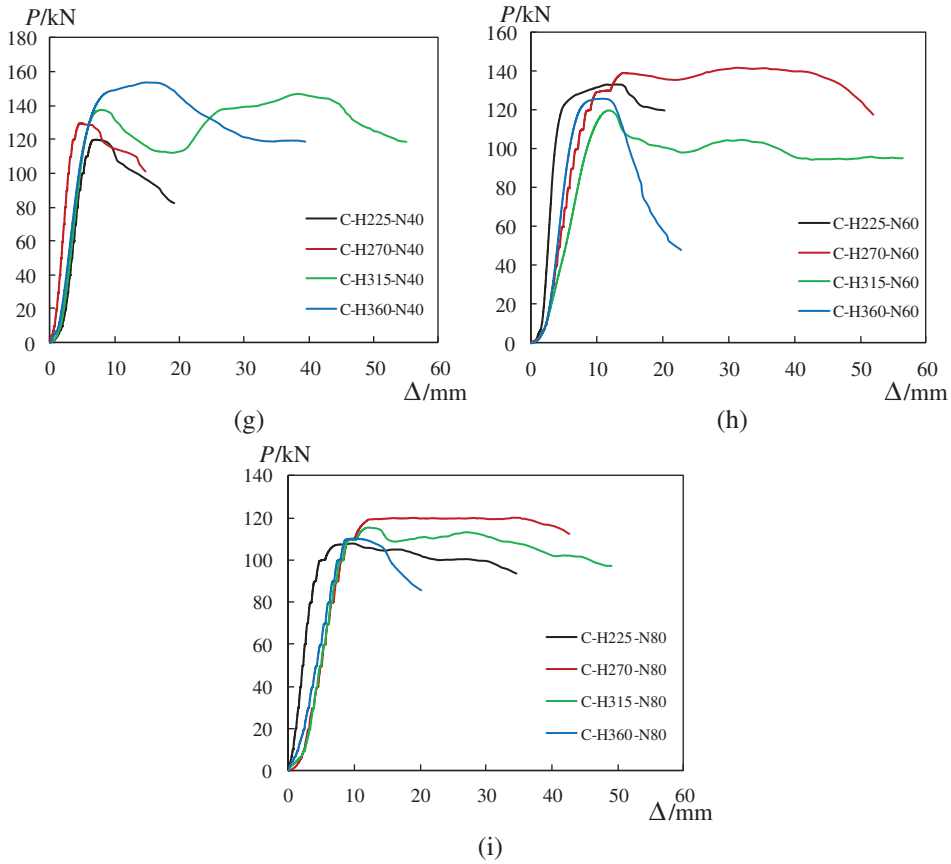

Figure 8: The load-displacement curves for circular timber columns. (a) H = 225 mm. (b) H = 270 mm. (c) H = 315 mm. (d) H = 360 mm. (e) N = 0. (f) N = 20. (g) N = 40. (h) N = 60. (i) N = 80

transverse and longitudinal strain of the specimen without being exposed to freeze-thaw cycles is corresponding greater than that of the specimens subjected to different number of freeze-thaw cycles in the mass. By contrast, the comparison of the strain among different number of freeze-thaw cycles shows that the effect of the number of freeze-thaw cycles on the strain is discrete; As to the corner area of the square specimens, the transverse and longitudinal strain of the specimens without being subjected to freeze-thaw cycles are smaller than that of the specimens subjected to freeze-thaw cycles except the specimen in the number of freeze-thaw cycles of 80 when the specimens were conducted to the same load. The ultimate value of the strain of the specimen without being exposed to freeze-thaw cycles is greater than that of the specimens subjected to freeze-thaw cycles. In addition, the growth rate of the strain of the specimen without being subjected to freeze-thaw cycles is greater than that of the specimens subjected to different number of freeze-thaw cycles except the specimen in the number of freeze-thaw cycles of 80. The specimens left untreated at ambient temperature have the biggest value of the strain than the specimens subjected to freeze-thaw cycles. Compared with the strain at the center of the specimens, the uptrend of the strain at the corner of the specimens is smaller with the increase of the load applied to the specimens, which indicates that the corner area of the specimens has better performance on anti-deformability than the center area of the specimens. It could also be found that the ultimate value of the transverse strain at the center or the corner of the specimens with different number of freeze-thaw cycles are respectively smaller than that of the longitudinal strain.

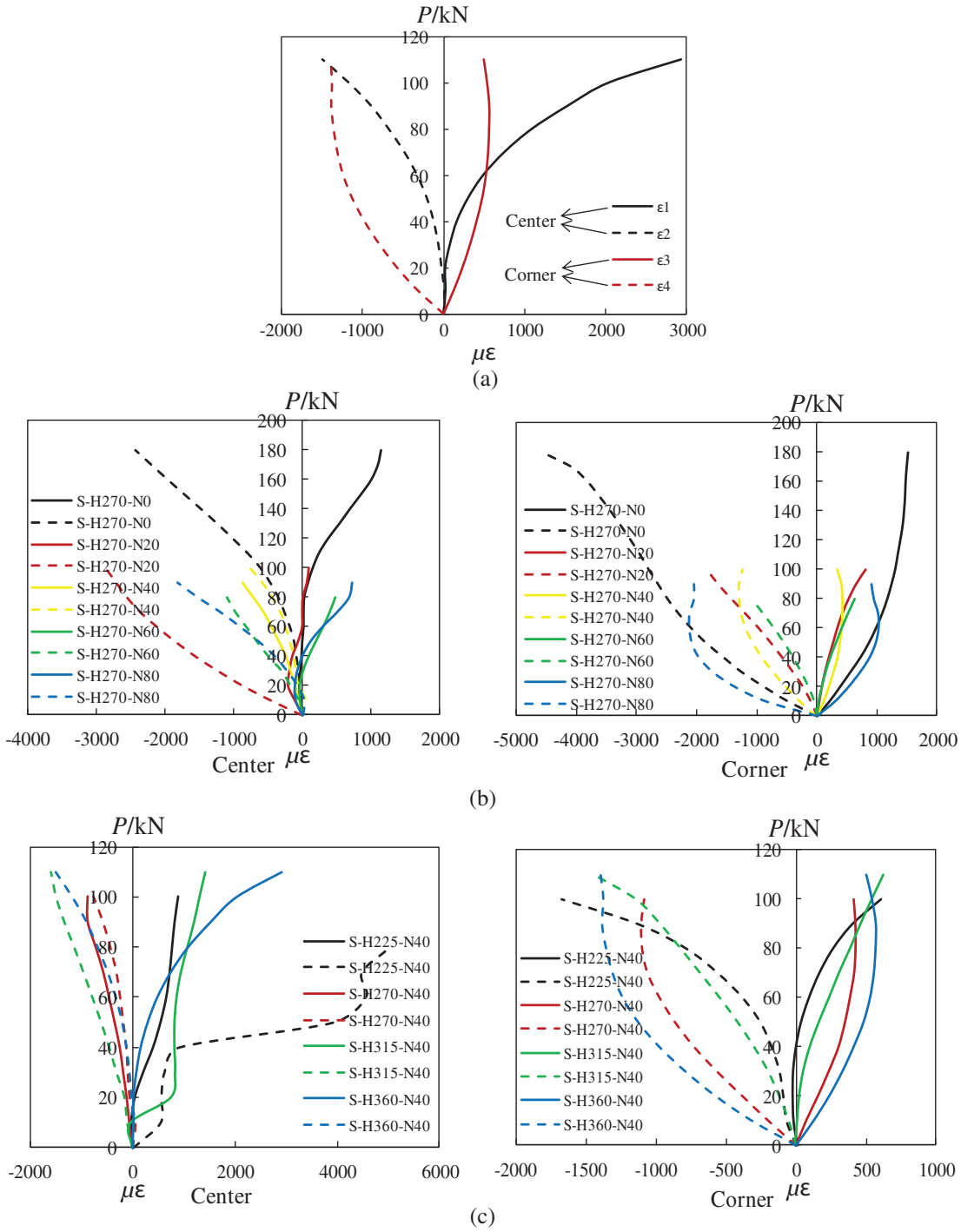

Figure 9: The load-strain curves for square timber columns. (a) S-H360-N40. (b) Different number of freeze-thaw cycles. (c) Different height of the square specimens

The load-strain curves of different height of the square specimens are shown in Fig. 9c. At the center of the specimens, the value of the transverse and longitudinal strain of the specimens with the height of 225 mm are all negative while the value of the transverse and longitudinal strain of the specimens with the height of

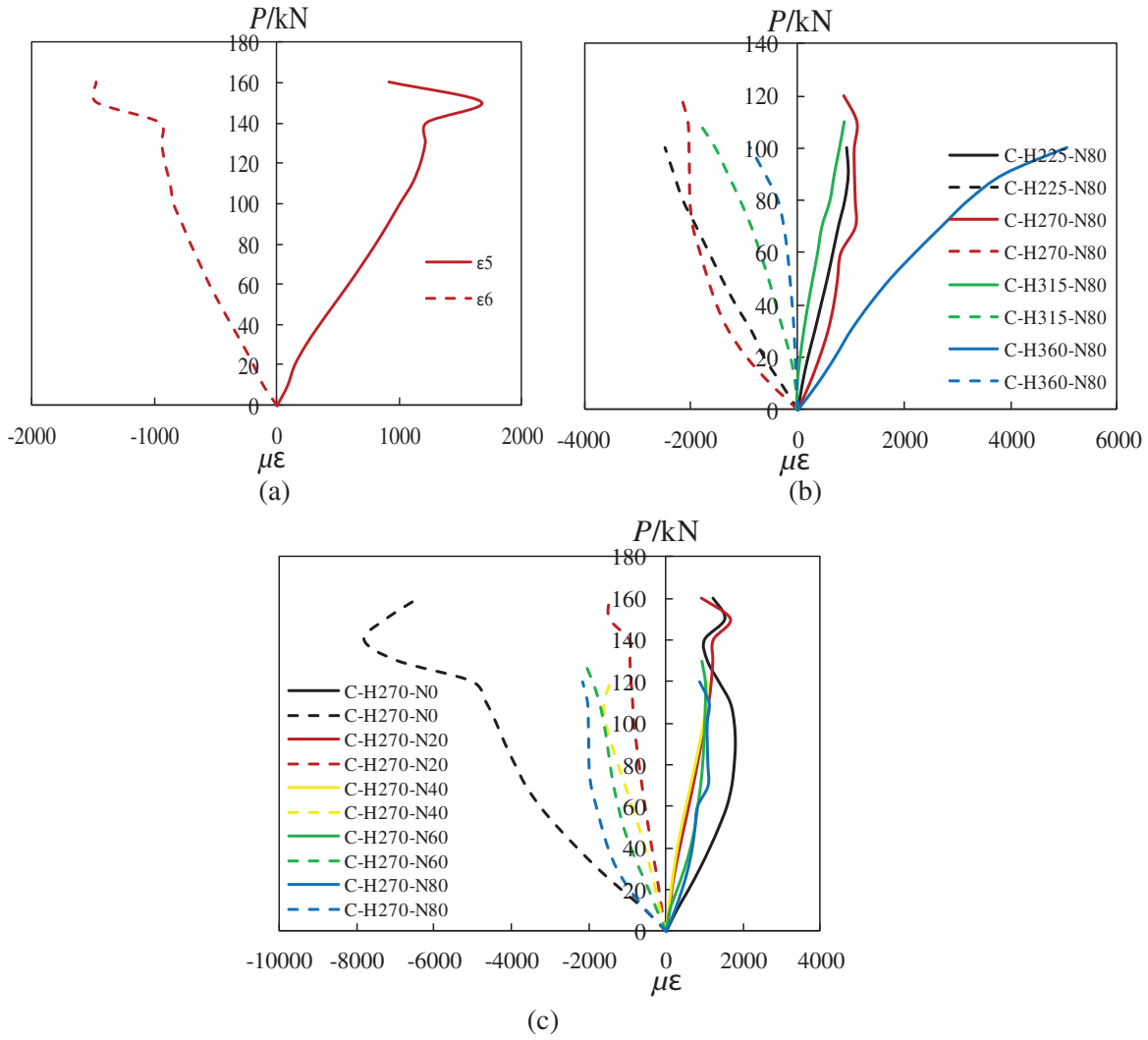

Figure 10: The load-strain curves for circular timber columns. (a) C-H270-N20. (b) Different height of the circular specimens. (c) Different number of freeze-thaw cycles

270 mm are all positive, which indicates that the destruction of the specimens with the height of 225 mm and 270 mm are mainly caused by instability of the specimens due to the fact that the value of the tensile strain is positive while the value of the compression strain is negative. Overall, the strain of the specimens subjected to freeze-thaw cycles increases with the increasing of the specimens' height ranging from 225 mm to 360 mm. As to the corner area of the square specimens with different heights, the growth rate of the strain of the specimens became greater with the increase of the specimens' height ranging from 225 mm to 360 mm, which indicates that, in the experimental range, the initial stiffness of the specimens became greater with the decrease of the specimens' height. With the increase of the specimens' height, the strain became greater when the specimens were at the same load levels. When it comes to the comparison between the longitudinal and transverse strains, it is found that the ultimate value of the longitudinal strain at the center of the specimens with different heights is smaller than that of the transverse strain. While the ultimate value of the longitudinal strain at the corner of the specimens with different heights is greater than that of the transverse strain.

The load-strain curves of different heights of the circular specimens subjected to freeze-thaw cycles are shown in Fig. 10b. It could be found that the longitudinal and transverse strains of the circular specimens with different heights have no consistent change, which shows that the effect of the specimens' height on the transverse and longitudinal strains of the circular specimens subjected to freeze-thaw cycles is discrete. It could also be seen from Fig. 10b that the growth rate of the strain of the specimen with the height of 270 mm subjected to the number of freeze-thaw cycles of 80 is greater than that of the specimens with the height of 225 mm, 315 mm and 360 mm in the mass when the specimens were subjected to the same load, which indicates that the initial stiffness of the specimen subjected to the number of freeze-thaw cycles of 80 in the height of 270 mm is worst when compared to the other specimens with different heights.

The load-strain curves of the circular specimens subjected to different number of freeze-thaw cycles are shown in the Fig. 10c. It could be found that the strain of the specimen without being exposed to freeze-thaw cycles has the greatest growth rate, and the growth rate of the strain of the specimens subjected to different number of freeze-thaw cycles increases with the increasing of the number of freeze-thaw cycles, which indicates that the initial stiffness of the specimens subjected to different number of freeze-thaw cycles decreases with the increasing of the number of freeze-thaw cycles. In addition, it could be seen that the greater the number of freeze-thaw cycles is, the larger the strain of the specimens subjected to freeze-thaw cycles is, when the specimens were at the same load levels.

4 Analysis of Test Results

The experimental results of the timber columns are shown in Tab. 3, in which the ultimate bearing capacity (N_u), yield load of the specimens (N_y), decline of the percentage in the ultimate bearing capacity of the specimens (*Per*), ultimate displacement (Δ_u), yield displacement (Δ_y) and the ductility coefficient ($\mu = \Delta_u/\Delta_y$) are gathered and analyzed. The Secant stiffness method, as shown in Fig. 11, is adopted to obtain the yield displacement (Δ_y) and yield load (N_y) of the specimens in this paper according to Chen et al. [32].

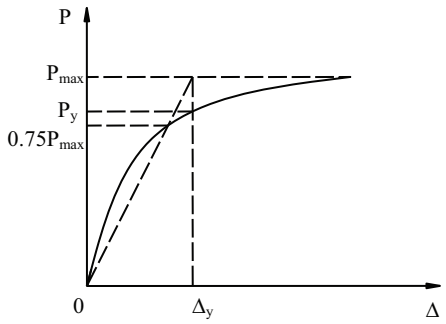

Figure 11: Secant stiffness method

4.1 Effect of the Number of Freeze-Thaw Cycles

Freeze-thaw cycles has a great impact on the mechanical performance of the timber columns, which could be proved according to Tab. 3, Figs. 7–14. As shown in Tab. 3, the ultimate bearing capacity of the specimens subjected to freeze-thaw cycles decreases sharply, and the decline of the percentage in the ultimate bearing capacity of the timber columns subjected to freeze-thaw cycles ranged from –3.4% to 54.0% when compared to that of the specimens at ambient temperature. Besides, the average decline of the percentage in the ultimate bearing capacity of the specimens subjected to freeze-thaw cycles is 28.0%, over one fourth of the decline of the percentage in the ultimate bearing capacity compared with the specimens left to be untreated. Therefore, it is obvious to get the conclusion that freeze-thaw cycles could shapely reduce the ultimate bearing capacity of the timber columns.

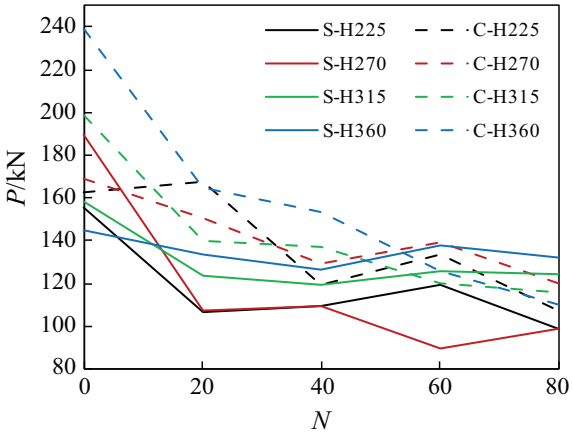

Figure 12: *P-N* curves

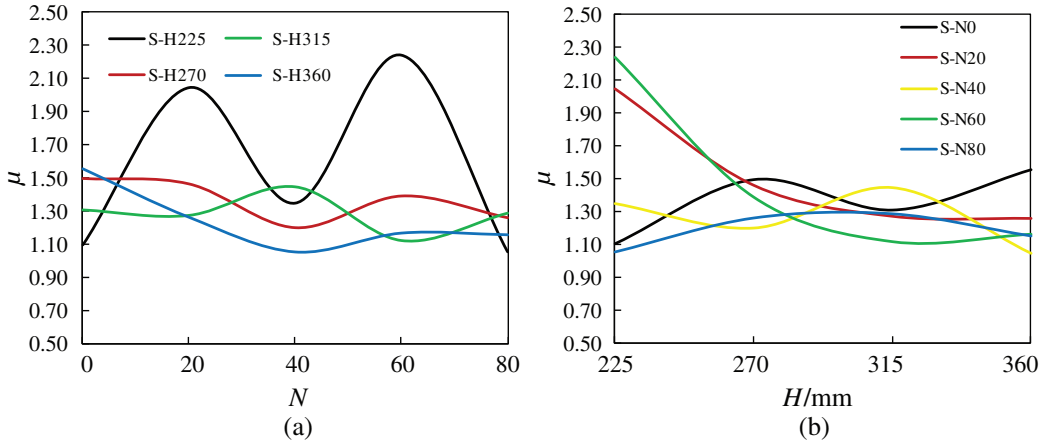

Figure 13: The effect of parameters on μ of the square timber columns. (a) μ-*N*. (b) μ-*H*

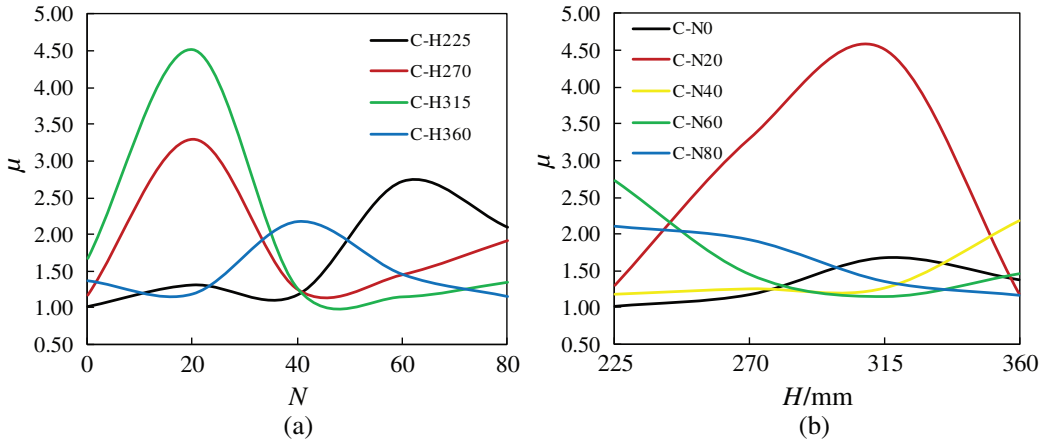

Figure 14: The effect of parameters on μ of the circular timber columns. (a) μ-*N*. (b) μ-*H*

The load-displacement curves of the timber columns with different freeze-thaw cycles are shown in Figs. 7 and 8. It is found that the freeze-thaw cycles reduced the initial stiffness of the timber columns in the mass whatever the section type of the timber columns is. For circular timber columns, the larger the specimens' height is, the more obvious the decline trend of the initial stiffness shows. In addition, the decent degree of bearing capacity of square specimens is observed to be maximum when the height of specimens is 270 mm. While the decent degree of bearing capacity of circular specimens increases with the increasing of the height of specimens.

The load-strain curves of the timber columns with different freeze-thaw cycles are shown in Figs. 9 and 10. It could be found that, at the center of square timber columns, the growth rate of the strain increases when the specimens were subjected to freeze-thaw cycles. While the growth rate of the strain at the corner of the specimens decreases when the specimens were subjected to freeze-thaw cycles, which indirectly indicates that the stiffness at the center and corner of the specimens subjected to freeze-thaw cycles are respectively better and worse compared with the specimens left untreated at ambient temperature. As for the circular timber columns, the growth rate of strain of the specimens at ambient temperature is found to be faster than that of the specimens subjected to freeze-thaw cycles, which shows that the stiffness of the specimens at ambient temperature are worse than that of specimens subjected to freeze-thaw cycles.

As to the influence of different number of freeze-thaw cycles on the ultimate bearing capacity of the timber columns, it could be summarized from Fig. 12. As it could be seen, on the whole, the ultimate bearing capacity of the timber columns decreases when the specimens were subjected to freeze-thaw cycles whatever the section type of the specimens is. It could also be found that the ultimate bearing capacity of the circular specimens are respectively larger than that of the square specimens whether the specimens were subjected to freeze-thaw cycles or not, which indicates that the circular timber columns have better axial compression resistance than the square timber columns. Moreover, with regard to the ultimate bearing capacity of the circular specimens, the range of descent is larger than that of the square specimens when the specimens were exposed to freeze-thaw cycles, which could be explained by the fact that the freeze-thaw cycles has worse influence on the ultimate bearing capacity of circular timber columns than that of square timber columns.

In Tab. 3, the ductility coefficient of all timber columns is shown, and the effect of freeze-thaw cycles on the ductility coefficient ($\mu = \Delta_u/\Delta_y$) of the specimens is presented in Figs. 13 and 14. For the square specimens, it could be found that the number of freeze-thaw cycles has little effect on μ of the specimens except the specimens with the height of 225 mm. As to the circular specimens, the effect of the number of freeze-thaw cycles on μ of the specimens is found to be discrete. However, the value of ductility coefficient of the specimens has an uptrend when the circular specimens were subjected to freeze-thaw cycles, which indicates that μ of the circular specimens could be promoted by freeze-thaw cycles. The difference in ductility of the two cross-section specimens is due to the difference in the effect of the components under the same freeze-thaw cycle. For a circular cross-section, the temperature transfer path is consistent from any point of the cross-section edge to the center, but there is a clear difference in the temperature transfer path of the square cross-section from the corner to the center of the side. This results in the freeze-thaw cycle effect on the circular cross-section specimen being more uniform than that on the square cross-section specimen. Therefore, there is a difference in ductility between the two specimens after freeze-thaw cycles. At the same time, the stress concentration at the corner of the square section will further amplify this difference.

4.2 Effect of Height of the Timber Columns

The influence of the height on mechanical performance of the specimens is analyzed as follows:

In Tab. 3 and Fig. 7, for the square timber columns, the ultimate bearing capacity of the specimens increases on the whole with the enlargement of the height, but the initial stiffness of specimens are

discrete; For the circular timber columns, in Tab. 3 and Fig. 8, the ultimate bearing capacity of the circular specimens at the number of freeze-thaw cycles in 0 and 40 increases with the enlargement of specimens' height while the ultimate bearing capacity is found to be irregular for the specimens at the number of freeze-thaw cycles in 20, 60 and 80. At the meantime, the specimens' height has little effect on the initial stiffness of the specimens.

In Fig. 9c, in general, the strain at the corner of square specimens increases with the increase of the height when the specimens were at the same load levels. The strain at the center of square specimens is found to be irregular with the change of the specimens' height. In Fig. 10b, the strain at the center of circular specimens is summarized to be discrete. As shown in Tab. 4, in the square specimens, when the slenderness ratio (λ) exceeds 10.39, the bearing capacity of the specimen (N_u) has a certain increase. However, in the circular specimens, the correlation between the bearing capacity and the slenderness ratio of the specimen is weak.

In Fig. 15, the ultimate bearing capacity of circular timber columns is shown to be always larger than that of square timber columns, respectively, which indicates that circular timber columns have better axial compressive property than square timber columns whether the specimens were subjected to freeze-thaw cycles or not. At the same time, it can be seen from Tab. 4 that for all square specimens except S-H360-N60, the compressive strength (N_u/A) of the specimens is less than 17 MPa, and the compressive strength of all circular specimens except C-H225-N80 and C-H360-N80 is greater than 18 MPa. Obviously, the compressive strength of the circular column is higher than that of the square column. Furthermore, the specimens' height is found to have little and irregular influence on the ultimate bearing capacity of the specimens.

As to the ductility coefficient (μ), in Figs. 13 and 14, for the square timber columns, the range ability of μ became small with the increase of height of specimens; for the circular timber columns, the range ability of μ is very gentle with the change of height except the specimens at the number of freeze-thaw cycles in 20.

4.3 Analysis of Variables

The effect of two parameters on V (Average value of Per) is shown in Figs. 16a and 16b. Compared with the specimens left untreated, the ultimate bearing capacity of square specimens with the height of 270 mm after being subjected to freeze-thaw cycles decreases greatest. The descend range of the ultimate bearing capacity of circular specimens after being subjected to freeze-thaw cycles increases with the increasing of specimens' height, as could be seen in Fig. 16a. Furthermore, the ultimate load bearing capacity of square specimens with different N after being subjected to freeze-thaw cycles decreases at the basically same degree compared with that of specimens left untreated. While the descend range of the ultimate bearing capacity of circular specimens after being subjected to freeze-thaw cycles increase with the increasing of N, as shown in Fig. 16b.

5 Theoretical Formulas

It could be seen that the ultimate bearing capacity of timber columns subjected to freeze-thaw cycles is mainly affected by the slenderness ratio (λ) of specimens and the number of freeze-thaw cycles (N). The ultimate bearing capacity of the timber columns (N_u) is given by following Eq. (1).

$$N_u = \frac{N_{au}}{K_i} \tag{1}$$

In Eq. (1), N_{au} and K_i are quoted and calculated by Eqs. (2) and (3).

$$N_{au} = \alpha \times f(\lambda)^2 + \beta \times f(\lambda) + \gamma \tag{2}$$

Table 4: Comparison between the calculated and practical value of the ultimate bearing capacity

Labels	N	A (mm^2)	λ	N_u (kN)	N_u/A (MPa)	N_{cu} (kN)	N_{cu}/N_u
S-H225-N20	20	8100	8.66	106.65	13.17	100.98	0.947
S-H225-N40	40	8100	8.66	109.50	13.52	101.53	0.927
S-H225-N60	60	8100	8.66	119.25	14.72	103.81	0.870
S-H225-N80	80	8100	8.66	99.10	12.23	108.04	1.090
S-H270-N20	20	8100	10.39	107.15	13.23	113.16	1.056
S-H270-N40	40	8100	10.39	109.20	13.48	113.78	1.042
S-H270-N60	60	8100	10.39	89.95	11.10	116.33	1.293
S-H270-N80	80	8100	10.39	99.15	12.24	121.08	1.221
S-H315-N20	20	8100	12.12	123.35	15.23	110.86	0.899
S-H315-N40	40	8100	12.12	119.35	14.73	111.47	0.934
S-H315-N60	60	8100	12.12	125.75	15.52	113.97	0.906
S-H315-N80	80	8100	12.12	124.10	15.32	118.62	0.956
S-H360-N20	20	8100	13.86	133.75	16.51	94.09	0.703
S-H360-N40	40	8100	13.86	126.70	15.64	94.60	0.747
S-H360-N60	60	8100	13.86	137.70	17.00	96.72	0.702
S-H360-N80	80	8100	13.86	132.10	16.31	100.67	0.762
C-H225-N20	20	6358.5	7.07	167.85	26.40	121.34	0.723
C-H225-N40	40	6358.5	7.07	119.45	18.79	107.04	0.896
C-H225-N60	60	6358.5	7.07	133.40	20.98	101.39	0.760
C-H225-N80	80	6358.5	7.07	107.65	16.93	86.64	0.805
C-H270-N20	20	6358.5	8.49	150.35	23.65	125.79	0.837
C-H270-N40	40	6358.5	8.49	129.35	20.34	110.98	0.858
C-H270-N60	60	6358.5	8.49	139.20	21.89	105.11	0.755
C-H270-N80	80	6358.5	8.49	120.00	18.87	89.82	0.748
C-H315-N20	20	6358.5	9.90	140.20	22.05	143.04	1.020
C-H315-N40	40	6358.5	9.90	137.10	21.56	126.19	0.920
C-H315-N60	60	6358.5	9.90	119.90	18.86	119.52	0.997
C-H315-N80	80	6358.5	9.90	115.60	18.18	102.13	0.883
C-H360-N20	20	6358.5	11.31	164.65	25.89	173.06	1.051
C-H360-N40	40	6358.5	11.31	153.50	24.14	152.68	0.995
C-H360-N60	60	6358.5	11.31	125.90	19.80	144.61	1.149
C-H360-N80	80	6358.5	11.31	109.95	17.29	123.57	1.124

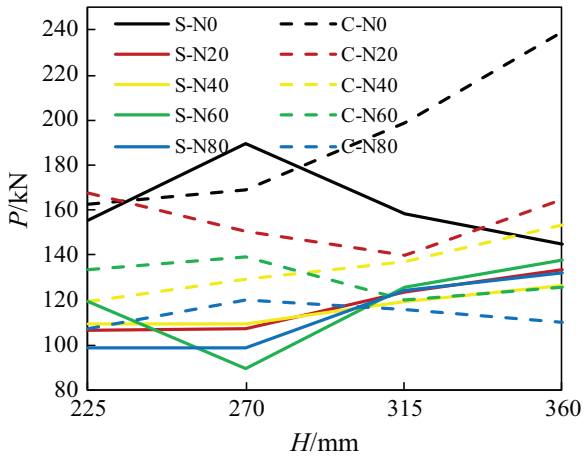

Figure 15: *P-H* curves

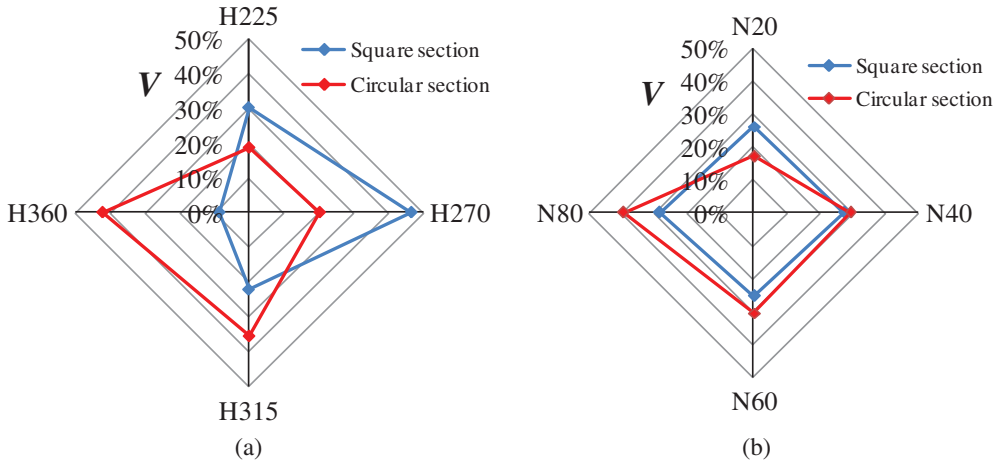

Figure 16: The effect of parameters on *V*. (a) Effect of height on *V*. (b) Effect of number of freeze-thaw cycles on *V*

$$K_i = \theta \times N^3 + \varphi \times N^2 + \psi \times N + \xi \tag{3}$$

where $f(\lambda)$ is the function of λ and calculated by Eq. (4)

$$f(\lambda) = f_c \times A \times \lambda \tag{4}$$

In these equations: λ is the slenderness ratio of specimens. A represents the cross section area of the specimens; N_{au} represents the theoretical ultimate bearing capacity without considering the number of freeze-thaw cycles of specimens; K_i is the impact factor of N on the ultimate bearing capacity of specimens; α, β, γ, θ, φ, ψ and ξ are the parameters of the function.

To verify the accuracy of the formula, the calculated ultimate bearing capacity was compared with the test, as shown in Tab. 4. In addition, the value of the parameters in the function is obtained by MATLAB, as shown in Tab. 5. For the square specimens, the minimum and maximum value of N_{cu}/N_u is 0.702 and 1.293, respectively. The mean value is 0.941 and the variance is 0.027. For the circular specimens, the minimum and

Table 5: The value of the parameters in the formula

Section type	$\alpha(\times10^{-4})$	β	γ	$\theta(\times10^{-6})$	$\varphi(\times10^{-5})$	$\psi(\times10^{-3})$	ξ
Square	–5.4	0.96084	–260.03590	0	–3	1.4	1.45220
Circular	9.0	–0.83383	331.10955	5	–70	35.6	0.6665

maximum value of N_{cu}/N_u is 0.723 and 1.149, respectively. The mean value is 0.941 and the variance is 0.017. Based on the analysis above, the formula is proved to be reasonable accuracy and conservative.

6 Conclusions

A total of forty timber columns with different heights subjected to different number of freeze-thaw cycles were tested in this paper. Based on the analysis of the experimental results, the conclusions are obtained as follows:

After exposure to freeze-thaw cycles, the size and appearance of the timber columns did not change significantly. Freeze-thaw cycles has no effect on the failure modes of the timber columns under axial pressure. When the slenderness ratio of the specimen exceeds a certain value, the probability of longitudinal penetration crack failure of the square specimen is significantly greater than the possibility of occurrence of oblique shear failure. The ultimate bearing capacity of timber columns decreased when the timber columns were subjected to freeze-thaw cycles, and the average reduction of the ultimate bearing capacity of the specimen reached 28%. The decline in the ultimate bearing capacity of circular timber columns is greater than the decline in the ultimate bearing capacity of square timber columns. The ductility coefficient of the square timber columns has no obvious change with the increase of the number of freeze-thaw cycles. As to the circular timber columns, its ductility coefficient increases when the specimens are subjected to freeze-thaw cycles overall. Based on the experimental results, the formula in calculating the ultimate bearing capacity of timber columns subjected to freeze-thaw cycles is derived, and the formula is proved to be accurate and conservative.

Acknowledgement: The author thanks Dr. Zhang and Dr. Guo for participating in the wood purchase for this study.

Funding Statement: This research work was supported by the National Natural Science Foundation of China (No. 51778066).

Conflicts of Interest: The authors declare that they have no conflicts of interest to report regarding the present study.

References

1. Esteves, B. M., Pereira, H. M. (2009). Wood modification by heat treatment: a review. *BioResources, 4(1),* 370–404.
2. Chung, K. F., Yu, W. K. (2002). Mechanical properties of structural bamboo for bamboo scaffoldings. *Engineering Structures, 24(4),* 429–442. DOI 10.1016/S0141-0296(01)00110-9.
3. Tian, L. M., Kou, Y. F., Hao, J. P. (2019). Flexural behavior of sprayed lightweight composite mortar-original bamboo composite beams: experimental study. *BioResources, 14(1),* 500–517.
4. Carlmark, A., Larsson, E., Malmstrom, E. (2012). Grafting of cellulose by ring-opening polymerization—a review. *European Polymer Journal, 48(10),* 1646–1659. DOI 10.1016/j.eurpolymj.2012.06.013.
5. Green, D. W., Evans, J. W., Logan, J. D., Nelson, W. J. (1999). Adjusting modulus of elasticity of lumber for changes in temperature. *Forest Products Journal, 49(10),* 82–94.
6. Moraes, P. D., Rogaume, Y., Bocquet, J. F., Triboulot, P. (2005). Influence of temperature on the embedding strength. *Holz als Roh-und Werkstoff, 63(4),* 297–302. DOI 10.1007/s00107-004-0568-9.

7. Adewopo, J. B., Patterson, D. W. (1999). Effects of heat treatment on the mechanical properties of loblolly pine, sweetgum, and red oak. *Forest Products Journal, 49(10),* 82–94.
8. Zhou, J. H., Hu, C. S., Hu, S. F., Yun, H., Jiang, G. F. et al. (2012). Effects of temperature on the bending performance of wood-based panels. *BioResources, 7(3),* 3597–3606.
9. Moya, R., Fallas-Valverde, L., Berrocal, A., Mendez-Alvarez, D. (2017). Durability of thermally modified wood of *Gmelina arborea* and *Tectona grandis* tested under field and accelerated conditions. *Journal of Renewable Materials, 5(3),* 208–219. DOI 10.7569/JRM.2017.634111.
10. Kim, M. H., Lee, S. M., Lee, J. M., Noh, B. J., Kim, W. S. (2010). Fatigue strength assessment of MARK-III type LNG cargo containment system. *Ocean Engineering, 37(14–15),* 1243–1252. DOI 10.1016/j.oceaneng.2010.05.004.
11. Ayrilmis, N., Buyuksari, U., As, N. (2010). Bending strength and modulus of elasticity of wood-based panels at cold and moderate temperatures. *Cold Regions Science and Technology, 63(1–2),* 40–43. DOI 10.1016/j.coldregions.2010.05.004.
12. Schmidt, R. A., Pomeroy, J. W. (1990). Bending of a conifer branch at subfreezing temperatures implications for snow interception. *Canadian Journal of Forest Research, 20(8),* 1250–1253. DOI 10.1139/x90-165.
13. Gerhards, C. C. (1982). Effect of moisture content and temperature on the mechanical properties of wood: an analysis of immediate effects. *Wood and Fiber Science, 14(1),* 4–36.
14. De-Geer, D., Bach, L. (1995). *Machine stress grading of lumber at low temperatures*. Edmonton: Alberta Research Council.
15. Gao, S., Wang, X. P., Wang, L. H. (2015). Modeling temperature effect on dynamic modulus of elasticity of red pine (*Pinus resinosa*) in frozen and non-frozen states. *Holzforschung, 69(2),* 233–240. DOI 10.1515/hf-2014-0048.
16. Tian, L. M., Kou, Y. F., Hao, J. P. (2019). Axial compressive behaviour of sprayed composite mortar-original bamboo composite columns. *Construction and Building Materials, 215,* 726–736. DOI 10.1016/j.conbuildmat.2019.04.234.
17. Szmutku, M. B., Campean, M., Porojan, M. (2013). Strength reduction of spruce wood through slow freezing. *European Journal of Wood and Wood Products, 71(2),* 205–210. DOI 10.1007/s00107-013-0667-6.
18. Juhl, H. B., Botfeldt, K. B., Andersen, L. B. (2012). The ability of waterlogged wood to resist freezing. *Proceedings of the 11th Icom Group on Wet Organic Archaeological Materials Conference, Greenville.*
19. Sonderegger, W., Niemz, P. (2013). Liquid water uptake from temporary frozen beech and spruce wood. *Holz als Roh-und Werkstoff, 9(4),* 601–606.
20. Grosse, C., Noel, M., Thevenon, M. F., Rautkari, L., Gerardin, P. (2018). Influence of water and humidity on wood modification with lactic acid. *Journal of Renewable Materials, 6(3),* 259–269.
21. Sparks, J. P., Campbell, G. S., Black, R. A. (2000). Liquid water content of wood tissue at temperatures below 0°C. *Canadian Journal of Forest Research, 30(4),* 624–630. DOI 10.1139/x99-241.
22. Barrett, J. D., Lau, W. (1991). Bending strength adjustments for moisture-content for structural lumber. *Wood Science and Technology, 25(6),* 433–447. DOI 10.1007/BF00225236.
23. Winandy, J. E. (1995). Effect of moisture-content on strength of CCA-treated lumber. *Wood and Fiber Science, 75 (6),* 168–177.
24. Kretschmann, D. E., Green, D. W. (1996). Modeling moisture content-mechanical property relationships for clear southern pine. *Wood and Fiber Science, 28(3),* 320–337.
25. Prokopski, G. (1996). Influence of moisture content on fracture toughness of wood. *International Journal of Fracture, 79(4),* R73–R77. DOI 10.1007/BF00018604.
26. Rammer, D. R., Winistorfer, S. G. (2001). Effect of moisture content on dowel-bearing strength. *Wood and Fiber Science, 33(1),* 126–139.
27. Pavlekovics, A., Niemz, P., Sonderegger, W., Molnar, S. (2008). Studies on the influence of wood moisture content on selected properties of particle boards and MDF. *Holz als Roh-und Werkstoff, 66(2),* 99–105. DOI 10.1007/s00107-007-0199-z.

28. Sedano-Mendoza, M., Navarrete, P., Pizzi, A. (2010). Effect of layers relative moisture content on the IB strength of pine tannin bonded particleboard. *European Journal of Wood and Wood Products, 68(3),* 355–357. DOI 10.1007/s00107-010-0452-8.
29. Jiang, J. L., Bachtiar, E. V., Lu, J. X., Niemz, P. (2017). Moisture-dependent orthotropic elasticity and strength properties of Chinese fir wood. *European Journal of Wood and Wood Products, 75(6),* 927–938. DOI 10.1007/s00107-017-1166-y.
30. Bader, M., Nemeth, R. (2019). Moisture-dependent mechanical properties of longitudinally compressed wood. *European Journal of Wood and Wood Products, 77(6),* 1009–1019. DOI 10.1007/s00107-019-01448-1.
31. Ministry of Housing and Urban-Rural Development of the People's Republic of China. (2009). Apparatus for resistance to freeze-thaw test of concrete.
32. Chen, Y., Wan, J., Wang, K., Han, S. H. (2017). Residual axial bearing capacity of square steel tubes after lateral impact. *Journal of Constructional Steel Research, 137,* 325–341. DOI 10.1016/j.jcsr.2017.06.019.